ELSEVIER

J. Non-Newtonian Fluid Mech. 131 (2005) 64–77

Journal of Non-Newtonian Fluid Mechanics

www.elsevier.com/locate/jnnfm

Rheological modelling of complex fluids: A transient network model with microstates

E. Rincón [a], A.E. Chávez [a], R. Herrera [a], O. Manero [b,*]

[a] *Facultad de Química, Universidad Nacional Autónoma de México, Ciudad Universitaria 04510, México D.F., Mexico*

[b] *Instituto de Investigaciones en Materiales, Universidad Nacional Autónoma de México, Ciudad Universitaria 04510, México D.F., Mexico*

Received 26 January 2005; received in revised form 23 June 2005; accepted 18 August 2005

Abstract

In this work, the dynamics of a transient network is analyzed with a model that includes two coupled kinetic processes to describe the rheological behavior of complex fluids. Five microstates are defined, representing the complexity of interactions among the macromolecules suspended in a Newtonian fluid. These microstates represent statistically networks with varying entanglement density, such as a dense entangled network in one extreme, and free chains or dangling ends (pendant chains) on the other extreme. It is assumed that the energy barrier required to modify the complexity of the system can be provided by flow, and that the flow-induced change in the network complexity is modelled as a coupled kinetic scheme constituted by a set of reversible kinetic equations describing the evolution of the microstates. The average concentration of microstates at a given time defines the maximum segment length joining the entanglement points in the transient network. The rheological material functions are calculated according to the classical statistical description of a transient network, but with a variable maximum segment length (variable extensibility), which is a function of the kinetics of the microstates. The model predicts shear banding in steady simple shear and time-dependent non-linear rheological phenomena, such as thixotropy, stretched exponential relaxation and other interesting responses of complex fluids.

Keywords: Transient network; Complex fluids; Kinetic process; Non-linear viscoelasticity

1. Introduction

The transient network model [1–3] envisages a polymer solution as a transient network defined by nodes and segments. The nodes are joined by polymer chains (segments) undergoing continuous collisions, due to thermal motion. The rheological behavior of the system depends on the kinetics of breakage and reformation of the network made of interacting polymer molecules suspended in a Newtonian fluid. The concentrated polymer solution is composed of a network of polymer molecules interacting each other at some specific sites along the molecules called junctions or nodes. In the transient network model formulation, the dynamics of segments joining the entanglement points is described statistically, in such a way that entanglements break and reform due to the deformation imposed by the applied flow.

The entropic force in the segments is modelled as the inverse Langevin function, and in some of these models the probability of segment breakage increases and diverges as the segments are stretched near to their maximum length. The segments evolution is simplified by replacing the exact entropic force law for each segment with an ensemble average. This "preaveraging" suggested by Peterlin [4] allows a closed set of equations to be derived for the stress tensor and the moments of the distribution function.

In this work, the maximum segment length, i.e., the critical length above which rupture of nodes occurs is not a constant but a variable resulting from a kinetic process describing the dynamics of various microstates. These microstates reflect the complexity of interactions among the polymer molecules in suspension, which can be free chains or pendant chains of the network, on one extreme, or the many-node interactions available in a dense network, on the other extreme. Within a statistical description, the properties of a system with a large amount of particles can be calculated by summation of the properties of each individual micro-system that comprises the entire system. The formal

* Corresponding author.
E-mail address: manero@servidor.unam.mx (O. Manero).

0377-0257/$ – see front matter © 2005 Elsevier B.V. All rights reserved.
doi:10.1016/j.jnnfm.2005.08.011

calculation of a property in a real system is a huge problem; an option is to propose an idealization to obtain an approximate solution.

Very simple microstates are defined representing all the possible structures that the transient network has when it is perturbed by an external force. The variation in the concentration of the microstates (creation and destruction of nodes in the network) is described by a system of coupled kinetic equations, such as the forward rate constants are function of temperature, as in thermally activated processes. The reverse rate constants, together with viscous dissipation due to flow, drive the system into a less entangled network. Variation in the number of nodes is calculated by defining an average dynamic distance between nodes, which represents the maximum elongation of the chains undergoing deformation. The distance between nodes is calculated as an average of the five basic microstates, which represent all the possible structures in the network.

The model is consistent with classical descriptions of transient networks. For example, when the concentration of free chains is large or when there is little structure modification due to the flow, the maximum segment length becomes constant with large magnitude. In this situation the system behaves as a Maxwell fluid, equivalent to a network of constant connectivity or a suspension of linear dumbbells.

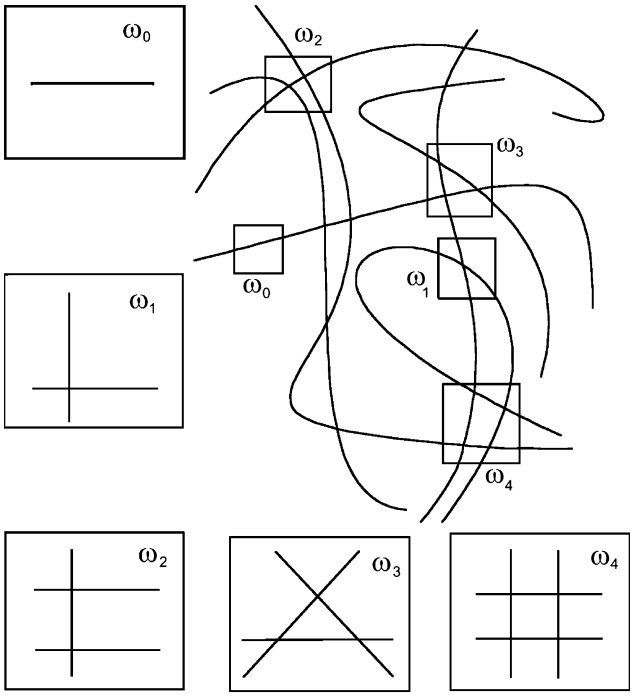

Fig. 2. The five basic microstates of a random arrangement of linear chains.

1.1. The model

The system is a transient network composed of a large group of flexible chains interacting as shown schematically in Fig. 1a. A node is defined as the point of physical interaction between two molecules, and a segment is the section of the molecule between nodes. The concept of node is equivalent to a physical entanglement forming the transient network. In Fig. 1b, the nodes, or points of contact between chains, are drawn and joined with straight lines. This composition gives rise to a mesh of triangles, squares or polygons, where the nodes represent the vertex points of these polygons and they are linked by segments of linear molecules. This network possesses statistically similar properties of the network shown in Fig. 1a, where the segment length is the average over that between nodes of polygons shown in Fig. 1b.

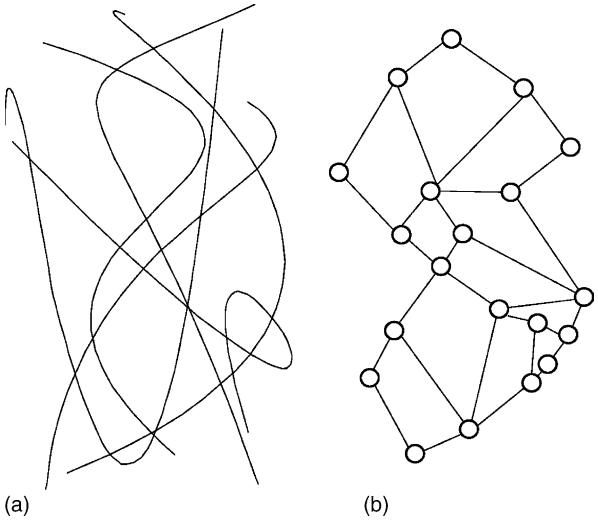

Fig. 1. Model of a random arrangement of linear molecules (a) and reduction to a non-regular polygon arrangements (b).

A microstate reflects the complexity of interactions amongst chains in a given region of space, and is defined in terms of the number of nodes. In Fig. 2, the microstates are schematically represented in a random arrangement of chains, and these give rise to five basic configurations shown in the same figure. Among the possible number of configurations available, the same number of nodes may represent microstates with different number of chains. However, a preferable state is that with the lower energy, which corresponds to that with a minimum number of chains.

In this approach, five microstates represent the possible configurations of the entire network, as illustrated in Fig. 2. In this form of representation, ω represents the specific microstate and the sub-index represents the number of nodes that define the microstate. For example, ω_0 represents a pendant (dangling end) or a free chain with no nearby interactions, as in a dilute system. ω_1 represents a configuration with one node and two chains. Similarly, three extra configurations are proposed, representing a more packed state with two, three and four nodes.

The next task is to calculate the average properties of the network considering these five microstates. Under a given deformation or flow, some microstates are favored, depending on the properties of the system represented by the network and also on the characteristics of the deformation process.

In terms of average quantities, let us define L_p, the maximum length of one extended free chain and $l'(t)$, which is the maximum end-to-end distance between nodes in the network (segments), including the dangling ends. By conservation of

Table 1
Microstate configurations and properties

Microstate	Geometry	Number of nodes	Number of segments	Number of chains	$l(t)$
ω_0		0	1	1	1
ω_1		1	4	2	$\frac{2}{4}=\frac{1}{2}$
ω_2		2	7	3	$\frac{3}{7}$
ω_3		3	9	3	$\frac{3}{9}=\frac{1}{3}$
ω_4		4	12	4	$\frac{4}{12}=\frac{1}{3}$

chains, the following relation arises:

$$(l'(t))\,(\text{number of segments}) = (\text{number of chains})\,(L_\text{p}) \tag{1}$$

The total length of the chains is the product of the length of one free chain multiplied by the number of chains. The number of chains is the product of the concentration of chains (C) in every microstate times the occupied volume of the chains (V). Similarly, the number of segments in the network is the product of the occupied volume times the concentration of segments in every microstate, including the dangling ends. Table 1 shows the geometry of every microstate and the number of nodes, segments and chains of each configuration. The number of chains is just the sum of products of the number concentrations of chains and a weighted factor in every microstate. Thus, the number of segments is the sum of products of segment concentrations and weighted factors in every microstate. Eq. (1) becomes:

$$l'(t) = \frac{VL_\text{p}(C_{\omega_0} + 2C_{\omega_1} + 3C_{\omega_2} + 3C_{\omega_3} + 4C_{\omega_4})}{V(C_{\omega_0} + 4C_{\omega_1} + 7C_{\omega_2} + 9C_{\omega_3} + 12C_{\omega_4})} \tag{2}$$

In terms of the non-dimensional distance between nodes, $l(t)$, Eq. (2) becomes:

$$l(t) = \frac{l'(t)}{L_\text{p}} = \frac{C_{\omega_0} + 2C_{\omega_1} + 3C_{\omega_2} + 3C_{\omega_3} + 4C_{\omega_4}}{C_{\omega_0} + 4C_{\omega_1} + 7C_{\omega_2} + 9C_{\omega_3} + 12C_{\omega_4}} \tag{3}$$

In the numerator we have the number concentration of chains of each microstate (column 5 of Table 1) and in the denominator we have the number of segments of every microstate (column 4 of Table 1). In addition, the non-dimensional average distance between nodes for every microstate is shown in column 6 of Table 1. The limits of $l(t)$ correspond to the situation where all chains are free ($l(t) = 1$) and that where all chains are in configuration ω_4($l(t) = 1/3$). Hence, the non-dimensional distance between nodes lies in the interval:

$$\frac{1}{3} \le l(t) \le 1 \tag{4}$$

The definition for the distance between nodes may also consider the case where a single chain may have various microstates. Then, the total length of the chain is divided by a large number of segments, giving rise to $l(t)$ values lower than 1/3. This case is not treated here at this stage of the model development.

The total number of nodes $n(\omega_i)$, can be obtained by summation of the products of the concentration of each microstate multiplied by the number of nodes of every microstate (column 3 of Table 1) times the total volume of the system:

$$n(\omega_i) = V(4C_{\omega_4} + 3C_{\omega_3} + 2C_{\omega_2} + C_{\omega_1}) \tag{5}$$

The description that follows considers that flow and properties of the system modify the concentration of microstates at a given time. A system of kinetic equations, similar to complex chemical kinetics, provides for the concentration of every microstate at time t. Since the network is transient, the number of nodes in the network is modified by flow or temperature. The transition between given microstates is described by reversible kinetics, where the forward "reaction" induces the formation of a more complex configuration (i.e., that with larger number of nodes) and the reverse "reaction" gives rise to a configuration with lesser number of nodes. The forward process is thermally activated, whereas the reverse process depends on the viscous dissipation.

1.2. Kinetic equations

The microstates are characterized by the number of nodes. Collisions between molecules subjected to Brownian diffusion and formation of physical entanglements require a state of thermal energy, which amounts to the energy of interaction between chains making a node. Under flow, the number of nodes decreases because the deformation energy overcomes the interaction energy between molecules involved in a node.

Table 2 shows the energy change involved in the process of modification of configurations or number of nodes. Conservation of chains is required for each transition. Let E_0 be the characteristic interaction energy corresponding to the energy associated in the collision between two molecules to form a junction or a single node.

In the first couple of transitions the change in energy corresponds to E_0 (see first and second rows in Table 2). As depicted in the second row, three single node configurations (six chains with energy content $3E_0$) give two double node configurations (six chains with energy content $4E_0$). The energy difference between these microstates is $\Delta E = E_0$. The total change in energy is $4E_0$. Similarly, in row three, a double node configuration (three chains with energy content $2E_0$) plus three single node configurations (six chains with energy content $3E_0$) give three triple node configurations (nine chains with energy content $9E_0$). The energy

Table 2
Energy change involved in structure transformations

Equation	Structure transformation	ΔE	ΔE_total
(6)		1	$E_1 = E_0$
(7)		1	$E_2 = 4E_0$
(8)	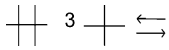	4	$E_3 = 9E_0$
(9)	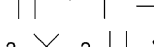	2	$E_4 = 12E_0$
(9B)	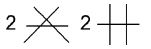	0	$E_\text{B} = 12E_0$

difference between the microstates is now $\Delta E = 4E_0$ and the total energy change is $9E_0$.

For the last transition we observe that microstate ω_4 can be obtained following two different paths. However, path 9B possesses zero energy difference, and as a consequence, the probability of its creation is the same as that for microstate ω_3. In this work, only one path for microstate ω_4 is considered (Eq. (9)).

In terms of the microstate transitions shown in Table 2, the following forward and reverse constants can be defined for each transition. In these equations, the forward rate constants (k^{A}) are the structure-formation kinetic quantities that have an Arrhenius dependence [5] with temperature, associated to a thermally activated process. The energy barrier is proportional to the energy change involved in the transition from one microstate into another, as disclosed in Table 2. The reverse rate constants (k^{B}) times the dissipation function represent the breakage or modification process of the transient network at a given time t. Then, the reverse process given by $k_i^{\mathrm{B}}\underline{\underline{\tau}} : \underline{\underline{D}}$ is a function of the stress level (flow strength) and type of flow through the velocity-gradient tensor. As the flow strength increases, one expects that the breakage process overcomes the reformation process, favoring microstates with low number of nodes. On the contrary, if the flow is weak, formation of more complex structures with larger number of nodes are preferred.

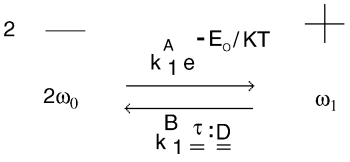

(6)

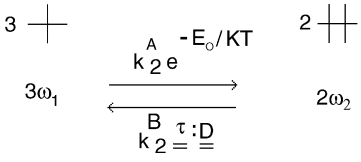

(7)

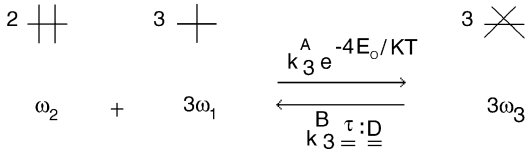

(8)

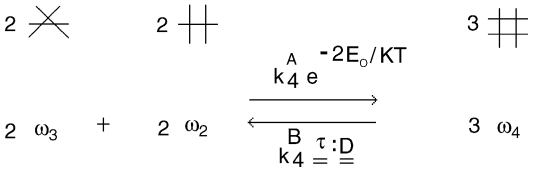

(9)

In equilibrium state, the temperature of the system is proportional to the number of nodes. As external forces act on the system, they modify the number of nodes and subsequently the system reacts to recover its equilibrium properties. The velocity of the recovery process is proportional to temperature through the Arrhenius equation and also is proportional to the constants $k_i^{\mathrm{A}}\mathrm{e}^{-(E_0/KT)}$. Following the method to write the kinetics of microstates as in complex chemical kinetics systems, we have:

$$\frac{\mathrm{d}C_{\omega_0}}{\mathrm{d}t} = \underline{\underline{\tau}} : \underline{\underline{D}}k_1^{\mathrm{B}}C_{\omega_1} - \mathrm{e}^{-(E_0/KT)}k_1^{\mathrm{A}}C_{\omega_0}^2 \tag{10}$$

$$\begin{aligned}\frac{\mathrm{d}C_{\omega_1}}{\mathrm{d}t} &= \mathrm{e}^{-(E_0/KT)}k_1^{\mathrm{A}}C_{\omega_0}^2 + \underline{\underline{\tau}} : \underline{\underline{D}}k_2^{\mathrm{B}}C_{\omega_2}^2 + \underline{\underline{\tau}} : \underline{\underline{D}}k_3^{\mathrm{B}}C_{\omega_3}^3 \\ &\quad - \underline{\underline{\tau}} : \underline{\underline{D}}k_1^{\mathrm{B}}C_{\omega_1} - \mathrm{e}^{-(E_0/KT)}k_2^{\mathrm{A}}C_{\omega_1}^3 \\ &\quad - \mathrm{e}^{-(4E_0/KT)}k_3^{\mathrm{A}}C_{\omega_2}C_{\omega_1}^3\end{aligned} \tag{11}$$

$$\begin{aligned}\frac{\mathrm{d}C_{\omega_2}}{\mathrm{d}t} &= \mathrm{e}^{-(E_0/KT)}k_2^{\mathrm{A}}C_{\omega_1}^3 + \underline{\underline{\tau}} : \underline{\underline{D}}k_3^{\mathrm{B}}C_{\omega_3}^3 + \underline{\underline{\tau}} : \underline{\underline{D}}k_4^{\mathrm{B}}C_{\omega_4}^3 \\ &\quad - \underline{\underline{\tau}} : \underline{\underline{D}}k_2^{\mathrm{B}}C_{\omega_2}^2 - \mathrm{e}^{-(4E_0/KT)}k_3^{\mathrm{A}}C_{\omega_2}C_{\omega_1}^3 \\ &\quad - \mathrm{e}^{-(2E_0/KT)}k_4^{\mathrm{A}}C_{\omega_2}^2C_{\omega_3}^2\end{aligned} \tag{12}$$

$$\begin{aligned}\frac{\mathrm{d}C_{\omega_3}}{\mathrm{d}t} &= \mathrm{e}^{-(4E_0/KT)}k_3^{\mathrm{A}}C_{\omega_2}C_{\omega_1}^3 + \underline{\underline{\tau}} : \underline{\underline{D}}k_4^{\mathrm{B}}C_{\omega_4}^3 \\ &\quad - \mathrm{e}^{-(2E_0/KT)}k_4^{\mathrm{A}}C_{\omega_2}^2C_{\omega_3}^2 - \underline{\underline{\tau}} : \underline{\underline{D}}k_3^{\mathrm{B}}C_{\omega_3}^3\end{aligned} \tag{13}$$

$$\frac{\mathrm{d}C_{\omega_4}}{\mathrm{d}t} = \mathrm{e}^{-(2E_0/KT)}k_4^{\mathrm{A}}C_{\omega_3}^2C_{\omega_2}^2 - \underline{\underline{\tau}} : \underline{\underline{D}}k_4^{\mathrm{B}}C_{\omega_4}^3 \tag{14}$$

where k_i^{A} and k_i^{B} are variable rate constants whose relative values are related to the energy content of the process. Many dynamic situations can be envisaged depending on the values of the rate constants. For example, some configurations or microstates may be more likely than others, giving rise to the possibility to predict flow-induced structuring of the system. Furthermore, time-dependent phenomena are also predicted, since the system of coupled Eqs. (10)–(14) are a function of time and the properties of the imposed flow. In this work, attention is restricted to simple situations where the rate constants can take values according to the difference in energy for each process shown in Table 2. The kinetic constants are given numerical values assuming that the ratio between them is equal to the energy ratio of each kinetic equation. Under these assumptions these constants are related as follows:

$$\begin{aligned}A &= k_1^{\mathrm{A}}\mathrm{e}^{-(E_0/KT)} = k_2^{\mathrm{A}}\mathrm{e}^{-(E_0/KT)} = 4k_3^{\mathrm{A}}\mathrm{e}^{-(4E_0/KT)} \\ &= 2k_4^{\mathrm{A}}\mathrm{e}^{-(2E_0/KT)}\end{aligned} \tag{15}$$

$$B = k_1^{\mathrm{B}} = k_2^{\mathrm{B}} = 4k_3^{\mathrm{B}} = 2k_4^{\mathrm{B}} \tag{16}$$

Substituting Eqs. (15) and (16) into Eqs. (10)–(14), the simplified system of kinetic equations can be written as follows:

$$\frac{\mathrm{d}C_{\omega_0}}{\mathrm{d}t} = B\underline{\tau} : \underline{\underline{D}}(C_{\omega_1}) - A(C_{\omega_0}^2) \tag{17}$$

$$\begin{aligned}\frac{\mathrm{d}C_{\omega_1}}{\mathrm{d}t} &= B\underline{\tau} : \underline{\underline{D}}\left[-C_{\omega_1} + C_{\omega_2}^2 + \frac{1}{4}C_{\omega_3}^3\right] \\ &\quad + A\left[C_{\omega_0}^2 - C_{\omega_1}^3 - \frac{1}{4}C_{\omega_2}C_{\omega_1}^3\right]\end{aligned} \tag{18}$$

$$\frac{dC_{\omega_2}}{dt} = B\underline{\underline{\tau}} : \underline{\underline{D}}\left[\frac{1}{4}C^3_{\omega_3} + \frac{1}{2}C^3_{\omega_4} - C^2_{\omega_2}\right] + A\left[C^3_{\omega_1} - \frac{1}{4}C_{\omega_2}C^3_{\omega_1} - \frac{1}{2}C^2_{\omega_2}C^2_{\omega_3}\right] \quad (19)$$

$$\frac{dC_{\omega_3}}{dt} = B\underline{\underline{\tau}} : \underline{\underline{D}}\left[\frac{1}{2}C^3_{\omega_4} - \frac{1}{4}C^3_{\omega_3}\right] + A\left[\frac{1}{4}C_{\omega_2}C^3_{\omega_1} - \frac{1}{2}C^2_{\omega_2}C^2_{\omega_3}\right] \quad (20)$$

$$\frac{dC_{\omega_4}}{dt} = \frac{B}{2}\underline{\underline{\tau}} : \underline{\underline{D}}[-C^3_{\omega_4}] + \frac{A}{2}[C^2_{\omega_3}C^2_{\omega_2}] \quad (21)$$

Several flow situations may be explored by assigning values to the overall kinetic constants A and B, based on experimental information. Summarizing, once the characteristics of kinetic equations of the system are defined according to experimental data, there are two constants to describe the behavior of the creation–destruction process of structures.

For example, the microstate representing a dilute system is ω_0. The series of constants describing the ω_0 configuration are:

$$A = k^{\mathrm{A}}_1 e^{-(E_0/KT)} = k^{\mathrm{A}}_2 e^{-(E_0/KT)} = k^{\mathrm{A}}_3 e^{-(4E_0/KT)} = k^{\mathrm{A}}_4 e^{-(2E_0/KT)} = 0 \quad (22)$$

$$B = k^{\mathrm{B}}_1 = k^{\mathrm{B}}_2 = k^{\mathrm{B}}_3 = k^{\mathrm{B}}_4 \geq 0 \quad (23)$$

In this case, the creation of nodes is absent as in a dilute system, because the probability of collision is too small. Consequently, only ω_0 is different from zero. The description of a dilute system involves the following initial conditions:

$$C_{\omega_1} = C_{\omega_2} = C_{\omega_3} = C_{\omega_4} = 0 \quad \text{and} \quad C_{\omega_0} \neq 0 \quad (24)$$

In contrast, for a concentrated solution, a specific number of microstates according to a particular concentration should be defined.

$$C_{\omega_0} = C_{\omega_1} = C_{\omega_2} = C_{\omega_3} = 0 \quad \text{and} \quad C_{\omega_4} \neq 0 \quad (25)$$

The concentration of the five microstates at time t determines the entanglement density of the network. The maximum length of segments between nodes ($l(t)$), is a dynamic average variable representing the concentration of given microstate configurations in a single parameter. To specify the dynamics of the segment end-to-end distance, a second kinetic process is proposed. This process follows the classical description of the dynamics of transient networks.

1.3. The distribution function

The classical description of the transient network [1–3] formulation assumes that the distribution function $\varphi(r,t)$ for the segments can be described by the equation.

$$\frac{\partial\varphi}{\partial t} + \nabla\cdot\dot{\underline{r}}\varphi = G - \beta\varphi \quad (26)$$

where G represents the rate of creation of the network junctions and β represents the rate of destruction of the network segments. $\dot{\underline{r}}$ is the rate of change of the end to end vector $\underline{r}$. As long as the chain remains Gaussian, the grand canonical function is defined as

$$\Omega = \left(\frac{L}{\sqrt{\pi}}\right)^3 e^{-L^2r^2} \quad (27)$$

with

$$L^2 = \frac{3}{2Nb^2} \quad (28)$$

In equilibrium, $G = \beta\varphi_0$. The equations for the moments of the distribution function, specifically, the second moment equations, can be obtained by multiplying Eq. (26) by $\underline{r}\,\underline{r}$ and averaging over the configuration space. The convected time derivative of $\underline{\underline{X}}$ is denoted by symbol $\overset{\nabla}{\underline{\underline{X}}}$, this leads to:

$$\langle\overset{\nabla}{\underline{r}\,\underline{r}}\rangle = \frac{1}{2}\beta L^{-2}\underline{\underline{\delta}} - \beta\langle\underline{r}\,\underline{r}\rangle \quad (29)$$

The creation function of the segments is Gaussian in equilibrium conditions, and the segments are modelled as entropic springs with elastic tension $\underline{F}$. The breakage process of segments is expected to be weakly dependent on chain extension, unless the chain becomes essentially fully stretched.

The elastic tension $\underline{F}$ in the chain varies linearly with the end-to-end distance $\underline{r}$ according to Hooke's law:

$$\underline{F} = H\underline{r} = \left(\frac{3KT}{Nb^2}\right)\underline{r} \quad (30)$$

where H is the elastic constant and b is the length of the Kuhn segment. The fully extended segment length is Nb, which in the present model is a dynamic variable $l(t)$. This linear law prevails as long as the tension $\underline{F}$ remains well under KT/b, a situation, which corresponds to an energy level much less than the energy barrier KT necessary to induce changes in the microstates; and hence, lower than the energy required for segment breakage.

In strong flows, the segments become almost fully stretched and hence the probability of segment breakage increases. In this model, the force follows the modified Warner [6] approximation of the inverse Langevin function, namely:

$$\underline{F}(\underline{r}) = -H\frac{\underline{r}}{1 - r^2/l(t)^2} \quad (31)$$

The end-to-end distance between nodes, $\underline{r}$, is bounded between the equilibrium value and the maximum end-to-end length ($Nb^2 < r^2 < l(t)^2$).

1.4. The moment equations

Under simple shear flow, the shear rate is given by $\dot{\gamma} = \partial V_x/\partial y$ (x is the flow direction and y is that of the velocity gradient), and therefore Eq. (29) leads to the following system of coupled differential equations for the components of the config-

uration tensor:

$$\frac{1}{\beta_0}\frac{\mathrm{d}\langle r_x r_x\rangle}{\mathrm{d}t} = \alpha\langle r_x r_y\rangle - \alpha\langle r_x r_x\rangle - h\langle r_x r_x\rangle + G \tag{32}$$

$$\frac{1}{\beta_0}\frac{\mathrm{d}\langle r_y r_y\rangle}{\mathrm{d}t} = -\alpha\langle r_x r_y\rangle - \alpha\langle r_y r_y\rangle - h\langle r_y r_y\rangle + G \tag{33}$$

$$\frac{1}{\beta_0}\frac{\mathrm{d}\langle r_z r_z\rangle}{\mathrm{d}t} = -h\langle r_z r_z\rangle + G \tag{34}$$

$$\frac{1}{\beta_0}\frac{\mathrm{d}\langle r_x r_y\rangle}{\mathrm{d}t} = \frac{\alpha}{2}[\langle r_y r_y\rangle - \langle r_x r_x\rangle] - h\langle r_x r_y\rangle \tag{35}$$

where h is given by

$$h = \frac{\beta(r)}{\beta_0} = \frac{1}{1 - r^2/l(t)^2} \tag{36}$$

β_0 is a constant and α is defined as

$$\alpha = \frac{\dot\gamma}{\beta_0} \tag{37}$$

The rate of segment creation G is therefore

$$G = \frac{Nb^2}{3} \tag{38}$$

Consistent with the above expression, the destruction function for the segments remains linearly dependent on the chain extension unless the chain becomes almost fully extended ($r \to l(t)$), when the destruction function diverges.

The stress tensor consistent with the force Eq. (31) is given by:

$$\underline{\underline{\tau}} = H\frac{1}{1 - r^2/l(t)^2}\langle \underline{r}\underline{r}\rangle + \eta_\infty\dot\gamma \tag{39}$$

where η_∞ is the limiting viscosity at very high shear rates, and it is usually of the order of the solvent viscosity.

As pointed out, the maximum end-to-end distance of the segments $l(t)$ is calculated from the kinetic Eqs. (10)–(14), which themselves are functions of the dissipation, and hence they are functions of the stress tensor. To start the calculations for a given flow, an initial condition for the variables should be given. The procedure to calculate the rheological material functions is described in detail later.

It is necessary to point out that the model proposes two different kinetics: one related to the dynamics of the microstates, which render the average maximum end-to-end distance of the segments $l(t)$, and the kinetics of breakage and reformation of the segments in the transient network. Other models proposed in the current literature, for example. Chilcott and Rallison [7] have examined the problem of variable maximum segment length, with interesting physical significance. Here, the kinetics of microstates is suggested to calculate such maximum length.

The system of Eqs. (32)–(35) in steady simple shear gives the following expressions [8] for the stress and normal stress differences:

$$\frac{\tau_{xy}}{H} = \frac{L}{\beta_0}\frac{\alpha}{h^2 - 4\alpha^2} \tag{40}$$

$$N_1 = \frac{L}{\beta_0}\frac{2\alpha^2}{h^2 - 4\alpha^2} \tag{41}$$

$$N_2 = -\frac{N_1}{2} \tag{42}$$

In steady simple-shear, the relation between stress and shear rate depends in a complicated manner on the kinetic constants A and B, which govern the breakage and reformation processes of the transient network. A depends on the Brownian motion through the Arrhenius expression and B represents the flow-induced modification of the microstructure. The dynamic balance of both constants governs the relative stability of the network as the system flows. It is convenient to define the non-dimensional ratios $A' = A/k_1^{\mathrm{A}}$ and $B' = B/k_1^{\mathrm{B}}$. To simplify the notation, constants A' and B' are written as A and B subsequently.

1.5. Method of solution

(A) For a given shear rate $\dot\gamma$, we select values for A and B to determine the breakage/reformation structural balance of the system. Values for the elastic constant H (proportional to the elastic modulus) and constant β_0 (inverse of the main relaxation time) in the second moment equations can be determined from known linear viscoelastic data. Given an initial stress, the kinetic equations are solved for a defined initial concentration of microstates, Eq. (25), for a concentrated system. For example,

$$C_{\omega_0} = C_{\omega_1} = C_{\omega_2} = C_{\omega_3} = 0, \qquad C_{\omega_4} = 25$$

Let us begin with 100 linear molecules corresponding to 100 microstates ω_0, or equivalently, 25 ω_4 configurations (see Table 1). Hence, $l(t)$ is equal to 1/3, according to Eq. (3).

(B) Microstate concentrations are calculated using Eqs. (17)–(21).

(C) For a given shear rate ($\dot\gamma$), β_0 and H, the segment elongations are calculated with the second moment Eqs. (32)–(35). The initial conditions for the equilibrium end-to-end distance at a given $\dot\gamma$ are $\langle \underline{r}\underline{r}\rangle_0 = Nb^2$.

(D) From known maximum segment end-to-end distances $l(t)$ and H, the stress components can be calculated using Eq. (39).

(E) The viscous dissipation is readily evaluated for shear flows:

$$\underline{\underline{\tau}} : \underline{\underline{D}} = \dot\gamma\tau_{xy} \tag{43}$$

(F) New values for the microstate concentrations can be calculated and an updated distance between nodes can be readily evaluated using Eq. (3).

(G) The segment end-to-end distance is updated, and subsequently, new values for the stress components are obtained.

(H) This calculation scheme is repeated from step B until a steady state value for the stress is obtained. The material functions (i.e., viscosity and normal stresses) are evaluated as well as the distance between nodes and the updated microstates concentrations.

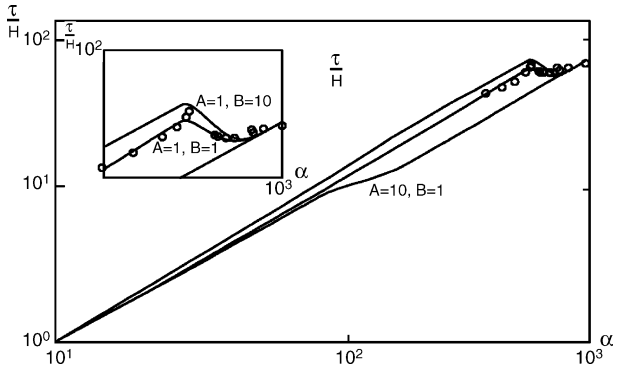

Fig. 3. Dimensionless shear stress vs. normalized shear rate ($\beta_0\eta_\infty/H = 0.08$). The inset shows an amplified window of the high shear rate region. Model predictions for various values of the parameters A and B: continuous lines. Experimental data of a telechelic (HEUR-type) associative polymer [9]: open circles.

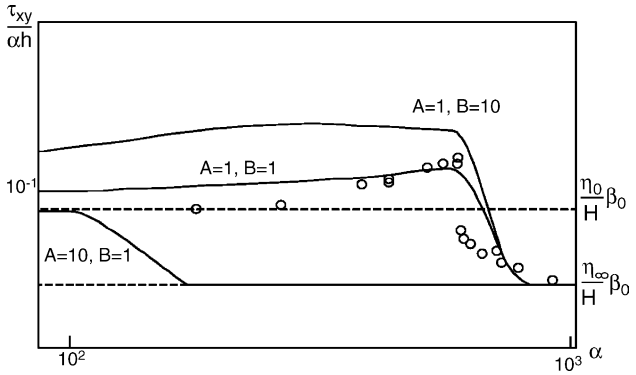

Fig. 4. Dimensionless shear viscosity vs. normalized shear rate. Model predictions: continuous lines. Experimental data [9] from Fig. 3: open circles.

Predictions of the present model include those of the classical network model (with constant maximum segment length). Hence, in Eq. (39), $l(t)$ is constant. This limit can be predicted assuming that:

1. The network resistance to flow deformation is high. In this case $B \to 0$ and the dissipation is negligible, i.e., $\dot{\gamma}\tau_{xy} \approx 0$. Eqs. (17)–(21) have solutions for $C_{\omega_0} = C_{\omega_1} = C_{\omega_2} = C_{\omega_3} = 0$ and $C_{\omega_4} \neq 0$.
2. The reformation of the network is carried out in a time scale shorter than that characterizing the flow. Distance between nodes tends to 1/3 for a wide range of shear rates. In this case, we assume that $A \gg B$.
3. The flow is weak, so that the energy associated with the deformation process is lower than that required to break the network.

In a working example, $l(t)$ constant requires, for example, a combination of large A and small B (i.e., 10 and 0.1, respectively) with the purpose to limit the network destruction and to extend the range of the linear regime, reproducing the Maxwell behavior with linear springs.

2. Results and discussion

2.1. Steady state

The steady state stress versus shear rate curves for several values of the constants A and B are shown in Fig. 3. In the inset, an enlargement of the region at high shear rates is reproduced. Experimental data by Berret et al. [9] of a telechelic associative polymer are shown in open circles.

These curves present extreme cases of the distance between nodes, i.e., between 1/3 and one. Newtonian or constant viscosity Maxwell behavior is represented by the curve predicted when the distance between nodes is sufficiently large so the segments end-to-end distances under flow are kept in the linear regime (as in a Hookean spring). The lower limiting curve ($A = 10$, $B = 1$) corresponds to the case when the distance between nodes remains equal to 1/3. This case belongs to classical network model predictions, where the largest distance between nodes is constant. In this case, for low shear rates, the behavior is Newtonian. Then the viscosity shear-thins and approaches a second linear region at high shear rates. A transition region between the linear and non-linear regimes as the shear rate increases is predicted. The critical stress for the onset of the non-linear regime depends on the network resistance to deformation by flow. The span of the linear regime rises as the largest end-to-end distance between nodes increases due to structure breakage, and hence the system supports increasing stresses within the linear regime.

Predictions are generated for various values of A and B. In all cases, for low shear rates, the system retains its structure and the behavior is Newtonian, coinciding with the case of fixed largest segment length. The effect of reducing the rate of reformation of the network or increasing the rate of flow-modification of the structure is to increase the stress level because the limiting distance between nodes increases with shear rate. A remarkable prediction is the multi-valued region at high shear rates, where for a given stress three values of the shear rate coexist (see inset). A maximum in the stress is predicted at a critical shear rate. This is the so-called “shear banding” regime, where bands of different shear rates appear at constant stress. Other viscoelastic constitutive equations show this strongly shear-thinning behavior corresponding to a plateau [10] in the shear stress–shear rate curve. Along the unstable range where the incremental viscosity is negative, various possibilities can be predicted: the flow takes very long times to become steady or may become inhomogeneous in space. Agreement of the predicted curve with $A = B = 1$ with experiments is apparent.

When plotted as shear viscosity versus shear rate, predictions and data in Fig. 4 describe a plateau (the first Newtonian viscosity) at low shear rates. Subsequently, past a critical shear rate, there is a power-law region, which ends into a second Newtonian plateau at high enough shear rates. The slopes of the power-law are -0.97 for ($A = 10$, $B = 0.1$), -1.38 for ($A = 1$, $B = 10$) and -1.62 for ($A = 1$, $B = 1$).

The latter region cannot be reproduced by the classical network models. A remarkable prediction observed between the Newtonian plateau and the shear-thinning [11] region is the shear-thickening regime when $l(t)$ approaches a constant value close to 1/3. In this case, the rate of structure rebuilding is shorter

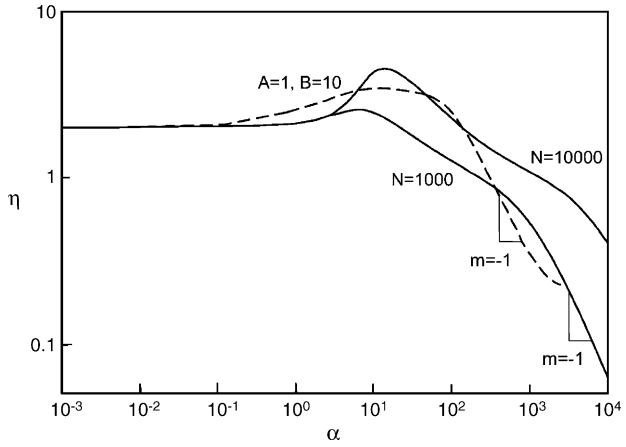

Fig. 5. Predictions of the model by Vaccaro and Marrucci [12] for two values of the parameter N (continuous lines) and those of the present model (broken lines) for $A = 1$ and $B = 10$. The slope m is indicated.

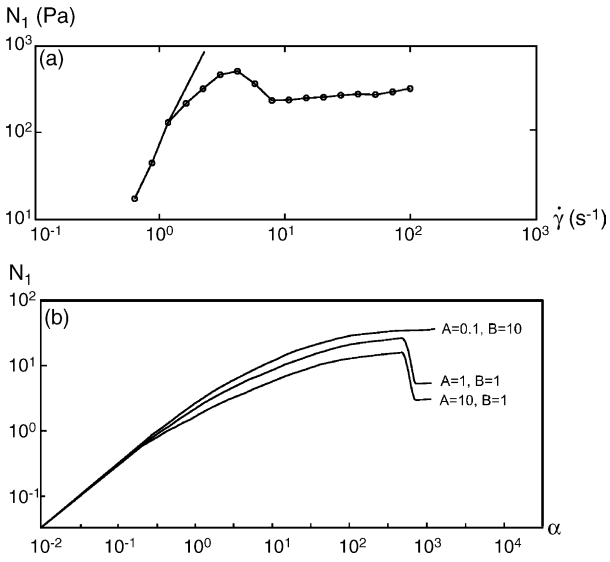

Fig. 6. (a) Experimental data [13] of the first normal stress difference vs. shear rate of a HEUR-type associative polymer. (b). Model predictions of the first normal stress difference vs. normalized shear rate for various values of the parameters A and B.

than the characteristic time of the flow, and hence a flow-induced structure prevails within a range of shear rates. For larger shear rates, the rate of network deformation overcomes its rate of reformation and degradation leads to shear-thinning. This effect has been observed in associative polymers and wormlike surfactants, and it has been predicted by Vaccaro and Marrucci [12]. Once again, quantitative agreement in the case of an associative polymer is found including the shear-thickening region prior to the pronounced shear-thinning.

In Fig. 5, predictions of the model by Vaccaro and Marrucci for associative polymers [12] (solid lines) are compared with those of the present model (broken lines). The shear-thickening region at low shear rates and the slope of minus one at high shear rates are predicted by both models. Notice that our model predicts a second Newtonian region at very high shear rates, which is not predicted by the Vaccaro and Marrucci model.

2.2. Normal stress differences

In Fig. 6a and b, data from Kaffashi et al. [13] for HEUR-type associative polymers (Fig. 6a) are compared with model predictions of the first normal stress difference as a function of shear rate (Fig. 6b).

Predictions do not cover the region of the quadratic dependence of N_1 at very low shear rates. N_1 attains larger values in the less structured network, as compared to those of the more elastic one. At low shear rates, the behavior of N_1 is quadratic with the shear rate (Maxwell limit) and the slope diminishes as the shear rate increases. An interesting prediction is the abrupt drop of N_1 at a critical shear rate, which is not predicted by the classical network models. This behavior at high shear rates is associated with predominant microstates of a less-entangled network (or broken network) past a critical shear rate. The systems that exhibit such behavior are those that present shear banding, where there is strong structure modification.

Since the normal stresses are associated directly with the elasticity of the network, it is consistent to relate the network rupture with the fall of the normal stresses. Notice that the model reproduces qualitatively the maximum exhibited in the data for two sets of parameters.

2.3. Stress relaxation after cessation of shear flow

Fig. 7 depicts the predictions of stress relaxation after cessation of steady shears flow for various shear rates ($A = 0.1, B = 10$). At very low shear rates, the relaxation time is 17.3 s when the non-dimensional shear rate is 1. At these low shear rates the relaxation approaches a single exponential behavior, characteristic of the Maxwell model. This behavior is predicted by network models with constant maximum segment length. In the cases shown in Fig. 7, single exponential behavior is attained at shear rates lower than 1. As the shear rate increases, two relaxation modes are observed: a short and a long relaxation. The short time relaxation is a function of the previous shear rate, while

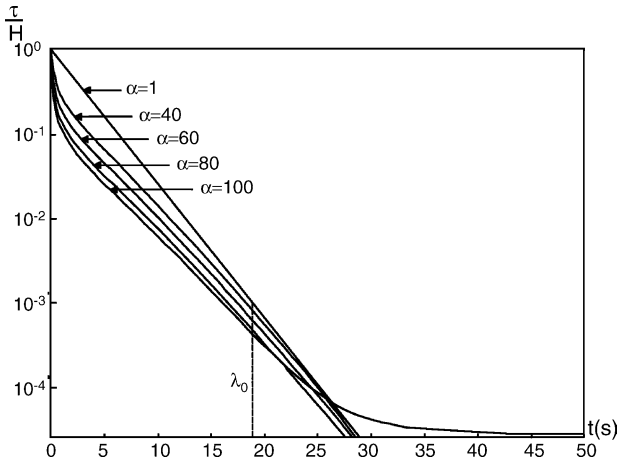

Fig. 7. Predictions of the stress relaxation after cessation of shear flow in a weakly structured network ($A = 0.1$, $B = 10$, $\lambda_0 = 18.8$ s), for various values of the normalized shear rate.

the long-time relaxation follows closely the longest (Maxwell) relaxation time. In Fig. 7, the long relaxation does depart from the Maxwell value and relaxation time increases, as the slope of the relaxation curves diminishes. A remarkable prediction is the complex behavior shown at high shear rates ($\alpha = 100$) for times longer than the Maxwell relaxation time. In this case, in addition to the short- and long-time relaxation modes, a curve following a stretched exponential [15] is predicted at long times, which would correspond to a spectrum of relaxation times. This behavior is ascribed to high breakage rate combined with a slow reformation rate of the network.

A limiting behavior is predicted as the shear rate increases in Fig. 7, in such a way that for larger shear rates a single limiting relaxation curve is obtained. This effect is associated to a saturation of the damping function at large shear rates, although the damping function is usually measured in stress relaxation experiments followed a step-strain. However, an estimation of the damping in stress relaxation analyzed here would correspond to the ordinate magnitude (extrapolation of the long-time stress relaxation curves to zero time) of the stress relaxation curves. The explanation of this limiting behavior may be ascribed to a maximum level of structure modification by flow, i.e., a dominant microstate ω_0. Two characteristic times govern the stress relaxation: the Maxwell time and the limiting time, which is consistent with the limiting behavior of the steady shear viscosity at low and high shear rates.

The stretched exponential behavior has been usually represented according to the following expression:

$$\frac{\tau_{xy}}{\tau_{xy}^{ss}} = \mathrm{e}^{-(t/\lambda_0)^{\varepsilon}} \tag{44}$$

Predictions of the stretched exponential region can be obtained with the following values of ε: 0.71 for ($A = 1$, $B = 10$), 0.61 for ($A = 1$, $B = 1$) and 0.768 for ($A = 0.1$, $B = 10$), which are very close to those values predicted for associative polymers or in wormlike micelle systems and in nanocomposites [16]. An example of the agreement is shown in Fig. 8, in which the stretched exponential region of the stress relaxation curve (broken line) is plotted with data of wormlike micelles by Berret et al. [14].

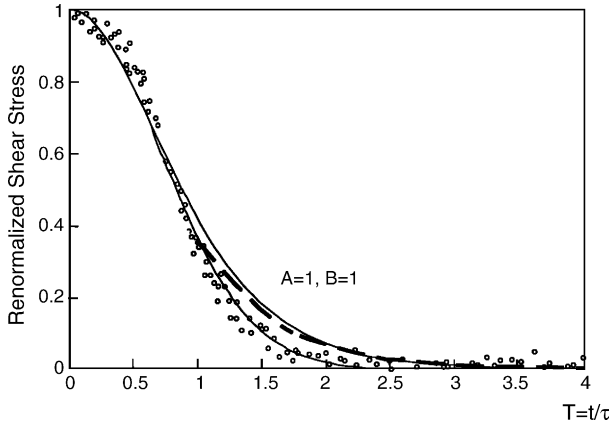

Fig. 8. Predictions of the stress relaxation after cessation of shear flow for a highly structured (flow-resisting) network ($A = 1$, $B = 1$, $\lambda_0 = 17.3$ s), showing the stretched exponential region (broken lines). Experimental data of a wormlike micellar solution [14]: open circles.

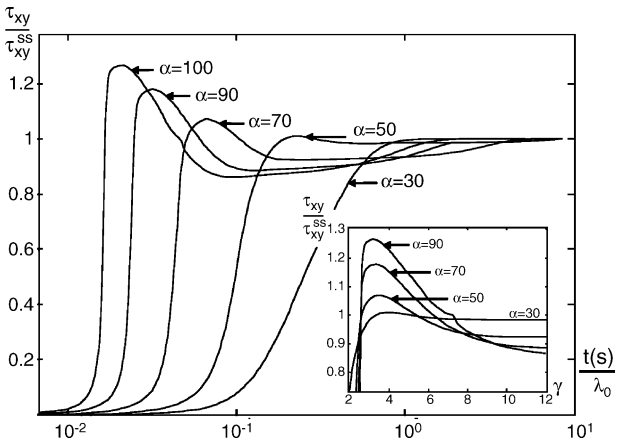

Fig. 9. Predictions of the stress growth upon inception of shear flow vs. time in a highly structured network ($A = 1$, $B = 1$) for various imposed shear rates. The inset shows the stress growth as a function of strain.

2.4. Stress growth upon inception of shear flow

Figs. 9 and 10 depict the stress response at the inception of shear flow for various imposed shear rates. Fig. 9 shows the non-dimensional stress versus reduced time for the case where $A = B = 1$. The stress is normalized by the value of the steady state stress, for imposed shear rates α between 30 and 100. For this case, which corresponds to a well-structured system, the behavior observed is that of a mono-exponential growth at sufficiently low shear rates. Overshoots are observed for increasing imposed shear rates, with maxima appearing at shorter times, similarly to polymer solutions and melts. As the shear rate increases beyond 50, overshoots followed by undershoots are predicted. For the largest applied shear rate 100 small oscillations superposed on the main curve are observed. This behavior may correspond to a highly non-damped system, where the effects of the elastic spring are dominant upon those of the medium viscosity. The kinetics of the microstates involves at each stage a degree of dissipation, which is responsible for the damped oscillations in this flow. Predictions for this case, where the maximum segment length departs little from the value of 1/3, corresponds closely to network models with constant maximum segment length. In the inset, the stress growth is plotted with strain, which leads to maxima located at almost the same value of strain (ca. 3), as observed in polymer solutions and melts. In this case the network maintains its structure with $l(t)$ around 1/3.

When the constants A and B are given values of 0.1 and 10, respectively, the stress growth is no longer monotonic for imposed shear rates α larger than 1, as observed in Fig. 10a. A relative maximum is observed at short times, followed by a minimum and a saturation at long times. The steady state value is larger than the overshoot value. In the inset, the stress growth versus strain shows that the first maxima is approximately located at the same strain and increase with shear rate. Steady state is attained at lower strains the larger the imposed shear rate.

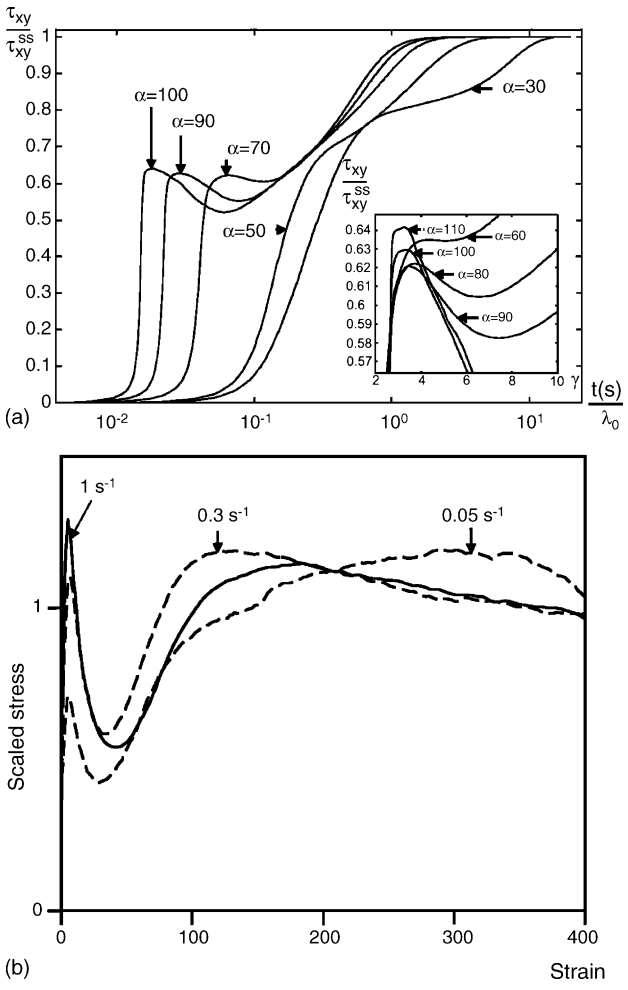

Fig. 10. (a) Predictions of the stress growth upon inception of shear flow vs. time in a weakly structured network ($A = 0.1$, $B = 10$) for various imposed shear rates. The inset shows the stress growth as a function of strain. (b) Experimental data [17] of the stress growth vs. strain are shown for various imposed shear rates of a viscoelastic emulsion.

Predictions depicted in Fig. 10a ($A = 0.1$, $B = 10$) correspond to a highly degradable network with slow reformation rate. Network breakage increases as compared to the previous case (Fig. 9) and the overshoots tend to fade. The elastic properties are overshadowed by increasing dissipation, and a trend to a less structured state is revealed.

In Fig. 10b, experimental data of stress versus time for various imposed strains from Lee and Denn [17] are shown. The system studied is a viscoelastic emulsion. As observed, the maximum at small strains is followed by a second maximum at large strains. The first maximum appears at the same strain and increases with imposed shear rate. Predictions in Fig. 10a show that the first maximum is approximately located at the same strain (see inset) and increases with shear rate, when the stress is plotted with strain. The second maximum in the data is shallow with small magnitude, whereas predictions of the model with the material parameters used show no maximum.

At the inception of shear flow, the maximum segment length changes with time, in a form that depends on the kinetic constants A and B. In Fig. 11, the maximum segment length $l(t)$ is plotted

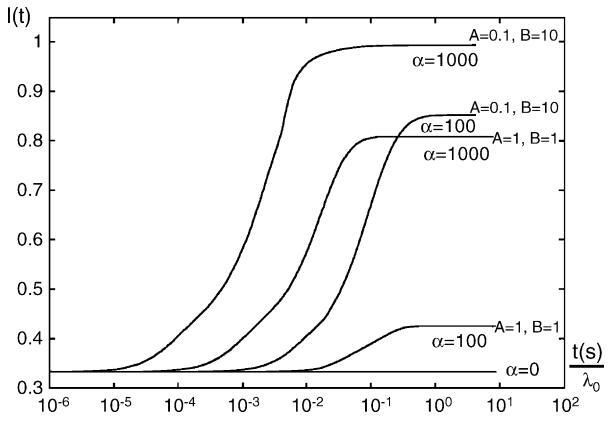

Fig. 11. Maximum segment-length as a function of time at the inception of shear flow, for various shear rates and several combinations of A and B.

with time for various shear rates. For low imposed shear rates in an entangled and flow-resistant network, $l(t)$ departs little from 1/3, which corresponds to the more entangled microstate, ω_4. To shift the maximum segment length to larger values (for instance, $l(t) = 0.8$) corresponding to less entangled microstates, it is necessary to apply much higher values of the shear rate ($\alpha = 1000$).

In the case of a less flow-resistant network ($A = 0.1$, $B = 10$) in which structure breakage dominates over structure rebuilding, small shear rates lead to less entangled microstates (ω_2 and ω_1), and hence to large values of $l(t)$. As shown in Fig. 11, steady values of $l(t)$ close to one are predicted with this network at shear rates of 100.

The nodes number as a function of the flow conditions can be obtained from the known microstate concentrations (Eq. (5)). In general, the number of nodes in the network decreases with increasing flow strength. As the applied shear rate is imposed, for most situations the relative number of nodes versus time goes through a minimum and thereafter levels off at long times, as shown in Fig. 12. For a loose network, the minimum is more pronounced and the equilibrium value of node concentration is lower for long times.

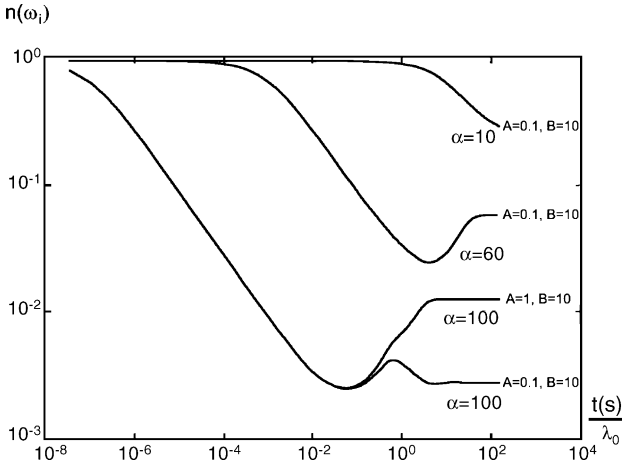

Fig. 12. Variation of the number of nodes as a function of time at the inception of shear flow for various shear rates and combinations of A and B.

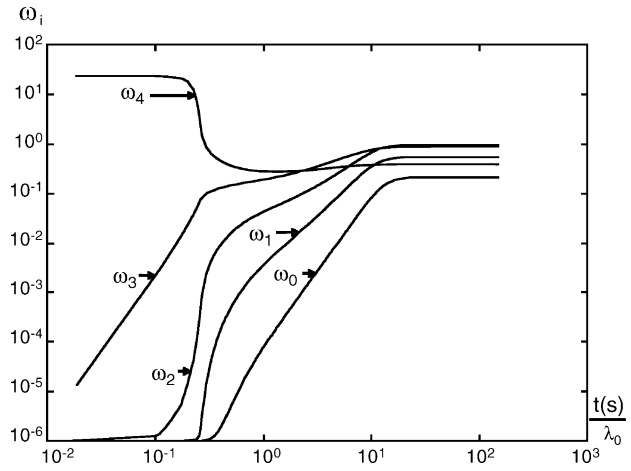

Fig. 13. Microstate concentrations as a function of time for a highly structured network at the inception of shear flow ($A = 1$, $B = 1$, $\alpha = 100$).

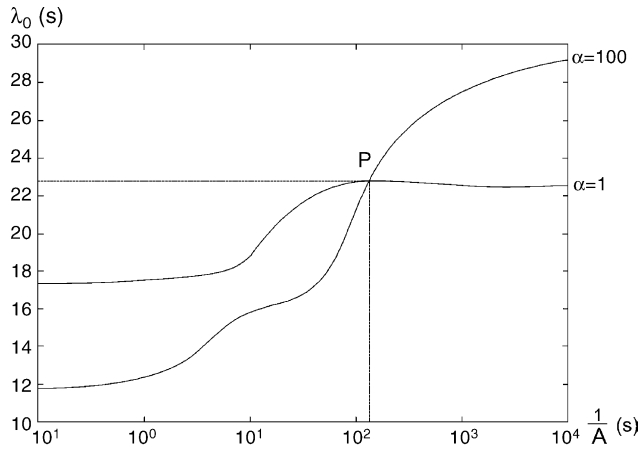

Fig. 15. Relaxation times predicted in stress relaxation after cessation of a slow and fast flows, respectively, as a function of the inverse forward kinetic constant A ($B = 10$).

In Figs. 13 and 14, the microstate concentrations for given flow conditions are shown, where the interplay between flow effects and network structure is clearly illustrated. Comparison between Figs. 13 and 14 shows that increasing dissipation and diminishing the rate of structure reformation leads to a change in the concentration of the dominant microstate. In the case where $A = B = 1$ (network reformation favored), concentrations of microstates ω_2 and ω_3 increase as a function of time and become dominant at long times for an applied shear rate α of 100. For the same shear rate, in the case illustrated in Fig. 14 ($A = 0.1$, $B = 10$) where network breakage is favored, ω_0 dominates at the expense of microstate ω_4. The physical significance of these results is that in networks where structure breakage is favored, a high proportion of free chains and low proportion of nodes are expected.

The kinetic constant A is related to the forward rate constants that drive the network into a more complex and structured system, and therefore is also related to the time scale of the rate at which the network reforms after the deformation process. The macroscopic relaxation time is thus also related to these processes. As soon as the deformation process is arrested, the network begins to rebuild by thermal motion. In this regard, it is interesting to compare the time scales of the reformation process and that of the relaxation time.

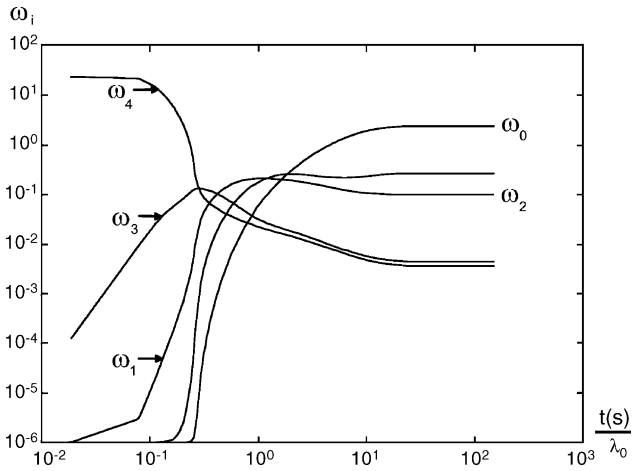

Fig. 14. Same as in Fig. 13 for a weakly structured network ($A = 0.1$, $B = 10$, $\alpha = 100$).

In Fig. 15, the main relaxation (Maxwell) time is plotted as a function of inverse A (which represents a time scale) for a fixed value of B and two shear rates. These shear rates are the extreme values shown in Fig. 7. The largest (Maxwell) relaxation time is predicted at low shear rates ($\alpha = 1$), and the limiting relaxation time is predicted at high shear rates ($\alpha = 100$). As the rate of network reformation increases with A, $1/A$ would give the time scale of the reformation process, which can be readily compared to the time scale of the stress relaxation process. When the shear rate is sufficiently small, within the linear viscoelastic (Maxwell) regime, a small change in the relaxation time is predicted throughout the range of $1/A$. On the other hand, for high shear rates, the variation of the relaxation time with $1/A$ is more accentuated. In fact, the relaxation time becomes shorter as the rate of rebuilding increases, but the ratio between the two processes is not linear, implying that they vary in different time scales. These differences are important in time-dependent experiments, when the rate of rebuilding of the structure is small (long times) but the stress relaxation is shorter. In this case, as the stress comes to zero and the system seems to be close to equilibrium, the structure has not reformed yet, and thixotropic phenomena may arise.

Another interesting aspect revealed in Fig. 15 is the prediction of relaxation times longer than those corresponding to linear viscoelasticity. The linear viscoelastic time (Maxwell time) is commonly referred to as the largest relaxation time in most systems. However, very large reformation times correspond to very low A, accompanied with relaxation times larger than those shown when the shear rate is very small. Point P signals the critical point where for smaller A, times longer than the Maxwell time are predicted.

The kinetic constant B refers to the backward rate constants that drive the network into a more disentangled microstate. It depends strongly on the viscous dissipation, and therefore is related to the processes that modify the state of the network.

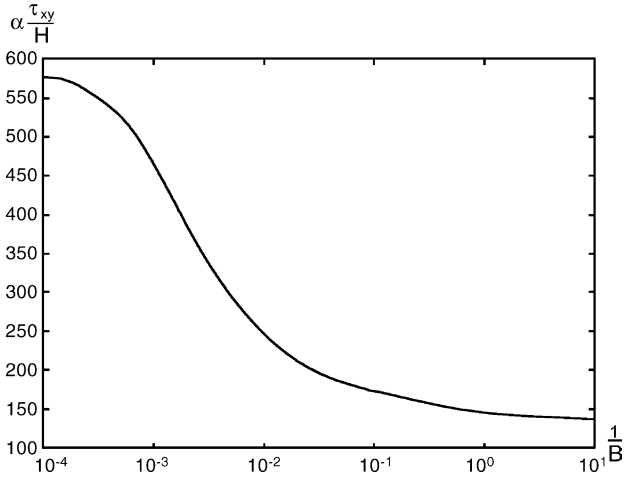

Fig. 16. Viscous dissipation as a function of the inverse kinetic constant B ($A = 10$).

Fig. 16 depicts the variation of the viscous dissipation $\alpha(\tau/H)$ as a function of inverse B. The curve presents two asymptotic regions at low and high B, with a regime of strong variation of B with viscous dissipation. In fact, the examples analyzed previously assigned values for B located in the low dissipation region. It would be interesting to explore higher dissipative systems corresponding to large values of B ($B > 10$).

2.5. Thixotropy

Time-dependent phenomena arise when the time scale of the reformation process after structure modification is different to that of the stress relaxation process. In this section we carry out transient flow predictions on networks with varying connectivity by assigning various values to the kinetic constants A and B. The imposed shear rate varies as a function of time, following a step-like increasing-and-decreasing deformation history or a continuous increasing-and-decreasing ramp of shear rates. Hysteretic curves are predicted for the stress versus shear rate for both deformation histories, as depicted in Figs. 17 and 18.

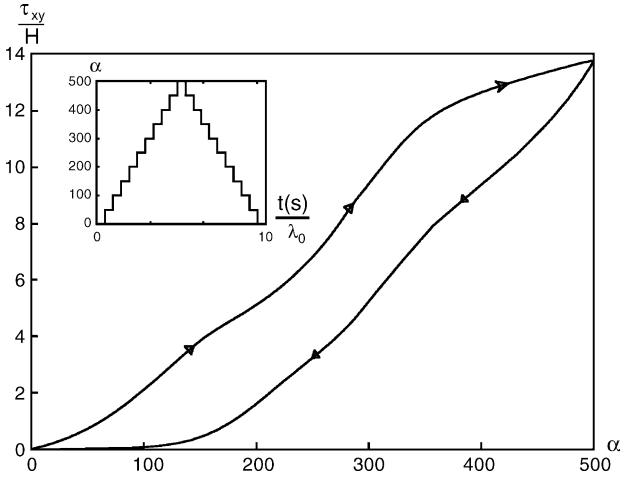

Fig. 17. Non-dimensional stress vs. normalized shear rate for a step-like ramp of ascending and descending shear rates, as shown in the inset ($A = 0.1$, $B = 10$).

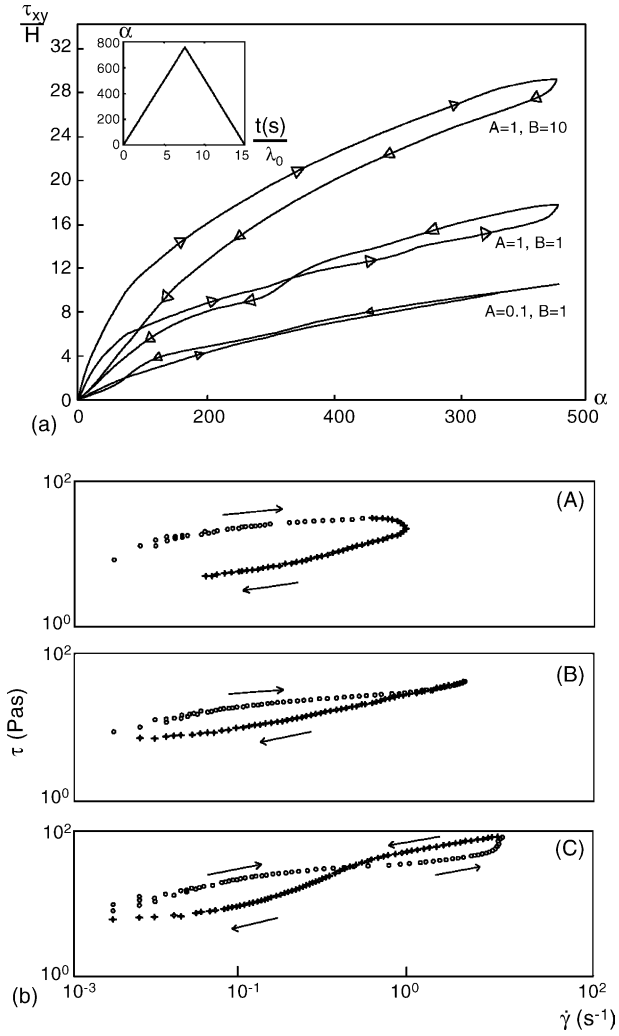

Fig. 18. (a) Non-dimensional stress vs. normalized shear rate for a continuous ramp of ascending–descending shear rates, as shown in the inset. Three different combinations of the kinetic constants are considered. (b) Experimental data [18] of lamellar liquid crystals.

Fig. 17 depicts the ascending and descending trajectory of the flow curve as a result of the imposed deformation history shown in the inset. The largest thixotropic area is predicted by reducing the time interval at each step to allow the rebuilding time (represented by A^{-1}) be larger than the relaxation time of the stress during that time interval. For the next increase in shear rate, the structure is not fully rebuilt and hence structure modification is increasing gradually at each step in shear rate. The accumulated breakage of the network leads to lower values of the stress in the descending path. This is a manifestation of the memory of past deformations in the system, which influences the present stress state. Highly dissipating networks favoring less entangled microstates lead to larger thixotropic areas in the flow curves, as shown in Fig. 17 where $A = 0.1$ and $B = 10$. A full analysis of the flow curves for various values of B reveals that this kinetic constant determines the hysteretic area of the flow curves.

In Fig. 18a, the flow history consists of a continuous increasing–decreasing ramp in shear rate. Three cases are ana-

lyzed, including a flow-resistant network ($A = B = 1$) and a network with large breakage rate of segments ($A = 1$, $B = 10$).

A remarkable prediction for the first case is the crossing of the flow curves; the ascending path lies above the descending curve, but this pattern reverses in the region of high shear rates. The pattern of the flow curves changes from a dominating anti-thixotropic ($A = 0.1$, $B = 1$) to a thixotropic one ($A = 1$, $B = 10$). The mixed thixotropic–anti-thixotropic pattern where the curves cross each other is predicted when $A = B = 1$. These flow patterns have been observed in lamellar liquid crystals and in other complex fluids. For example, in Fig. 18b, data is shown on the time-dependent behavior of surfactant-based lamellar liquid crystals [18], illustrating the transition from a thixotropic to an anti-thixotropic behavior. The model is able to capture the thixotropic loop and also the transition to the anti-thixotropic loop. The mixed loops are also predicted.

3. Concluding remarks

This model has been developed on the basis of a transient network formulation in which the instantaneous distance between nodes is calculated from the average over all structures presents in a given time. The complex interactions among the molecular chains are represented by a group of five microstates, which are functions of temperature and viscous dissipation.

The average distance between nodes is calculated from the individual contributions of each microstate at a given time. Five basic microstates are defined to include the most representative ways of chain interaction in a complex system. Consideration of complex structures in addition to the general two-chains/one-node microstate has several implications. Microstates with more than two chains can provide, to a first approximation, the existence of a more entangled (or structured) network. The reason to go beyond microstate two (that involving three chains) is to allow the possibility of a three-chain contact besides the more probable two-chain contact. There are various examples in kinetic theory of simple systems in which three-body collisions are included besides the two-body collisions. However, there is indeed a reason to limit the number of microstates in the model. The segment length (distance between nodes) is the same for configurations with more than three nodes, as described in Eqs. (2) and (3). From the ratio of the number of chains to the number of segments of a given microstate, it is not possible to go beyond 1/3 in a simple topology (excluding loops or cycles). This is, $l(t)$ in Eq. (3) will attain values of 1/3 when three chains arrange themselves in a microstate with nine segments (three nodes), and four chains will arrange in a microstate with 12 segments (four nodes) and so on. The reason of this result is that the energy involved in the generation of a given microstate is the same for microstates with more than three nodes, and hence configurations with more than three nodes influence equally the calculation of the stress in the transient network.

The concentration of every microstate is described by a system of kinetic equations in which the forward kinetic constants drive the system into a more complex structure, whereas the reverse kinetic constants determine the rate of structure breakage or modification due to the flow. The association probability of a given microstate is influenced by previous associations through a complex kinetic system of equations. The dynamics of the microstates depends on flow and the thermal state of the system.

To understand the relations among the kinetic constants is important to assume that the energy difference of each process, which leads to a given microstate (see Table 2, where the energy difference for each process is ΔE) is proportional to the magnitude of rate constants and that the constants ratios are unchanged. This is, the ratio of the forward rate constants times the exponential term is equal to the energy difference of each kinetic process. These assumptions lead to Eq. (15). In the same form, the ratio of the backward kinetic constants is equal to the energy difference of each kinetic process, which leads to Eq. (16). Since we deal with systems in which no chemical reactions occur, the "kinetic constants" should not be widely different to each other, and the assumptions made are not inconsistent with real complex kinetics.

In the present model, it is assumed that thermal motion only contributes to structure formation. However, it may also contribute to node destruction, and detachment can also be thermally activated. Although such contributions can also be incorporated in the model, here we assume that the flow strength has a larger effect on node destruction than that of the thermal motion. This is in agreement with transient network model formulations proposed by Green and Tobolsky [2], Yamamoto [3] and Vaccaro and Marrucci [12].

To incorporate in the model the notion of variable maximum segment length, the Warner expression for the entropic force is modified, in which this variable is a function of the concentration of the five basic microstates. The distance between association points along the polymer chain is one of the main ingredients of the model. $l(t)$, the non-dimensional distance between associations points, as given in Eq. (3), is the average ratio of the segments concentration with respect to the number of chains, and depends on the dynamics of the microstates. This distance changes according to flow strength and thermal motion.

Some of the remarkable predictions of this model include shear banding flow under steady state conditions, shear-thickening of the viscosity followed by shear-thinning, stretch exponential behavior in stress relaxation at long times, non-monotonic growth of the stress with time after inception of shear flow, and the variety of hysteretic curves (thixotropic and anti-thixotropic behavior) under transient deformation histories. Particular cases of the model include those where the maximum segment length is constant, corresponding to classical transient network models.

Acknowledgement

Support from CONACYT through project NC-204 is gratefully acknowledged.

References

[1] A.S. Lodge, Trans. Faraday Soc. 52 (1956) 120.
[2] Green, Tobolsky, J. Chem. Phys. 14 (1946) 80.

[3] M. Yamamoto, J. Phys. Soc. Jpn. 11 (1956) 413;
M. Yamamoto, J. Phys. Soc. Jpn. 12 (1957) 1148;
M. Yamamoto, J. Phys. Soc. Jpn. 13 (1958) 1200.
[4] A. Peterlin, Polymer 2 (1961) 257.
[5] R.E. Weston, H.A. Schwartz, Chemical Kinetics, Prentice Hall Inc., 1972.
[6] H.R. Warner, Ind. Eng. Chem. Fundam. 11 (1972) 3.
[7] M.D. Chilcott, J.M. Rallison, J. Non-Newtonian Fluid Mech. 29 (1988) 381.
[8] J. Zaragoza, O. Manero, Rev. Mex. Fís. 33 (1987) 49.
[9] J.F. Berret, Y. Serero, B. Winkelman, J. Rheol. 45 (2001) 477.
[10] F. Bautista, J.F.A. Soltero, H. Pérez-López, J.E. Puig, O. Manero, J. Non-Newtonian Fluid Mech. 94 (2000) 57.
[11] G. Marrucci, S. Bhargava, S.L. Cooper, Macromolecules 26 (1993) 6483.
[12] A. Vaccaro, G. Marrucci, J. Non-Newtonian Fluid Mech. 92 (2000) 261.
[13] B. Kaffashi, M. Barmar, J. Eyvani, Colloids Surf. A: Physicochem. Eng. Aspects 254 (2005) 125.
[14] J.-F. Berret, D.C. Roux, G. Porte, J. Phys. II France 4 (1994) 1261.
[15] Y. Séréro, V. Jacobsen, J.-F. Berret, Macromolecules 33 (2000) 1841.
[16] Q. Zhang, L.A. Archer, Langmuir 18 (2002) 10435.
[17] H.S. Lee, M.M. Denn, J. Rheol. 43 (1999) 1583.
[18] J.F.A. Soltero, O. Robles-Vasquez, J.E. Puig, O. Manero, J. Rheol. 39 (1995) 235.